A discussion on some relevant aspects for the experimental and numerical analysis of floating wind turbines based on a test case

Lucas H. S. Carmo[a,*], Pedro C. de Mello[a], Renato M. Monaro[a] and Alexandre N. Simos[a]

[a]University of São Paulo, Av. Prof. Mello Moraes, 2231, São Paulo, 05508-030, Brazil

ARTICLE INFO

Keywords:
Floating wind turbines
Model tests
Numerical modeling
Software-in-the-loop

ABSTRACT

A Lorem ipsum dolor sit amet, consectetuer adipiscing elit. Ut purus elit, vestibulum ut, placerat ac, adipiscing vitae, felis. Curabitur dictum gravida mauris. Nam arcu libero, nonummy eget, consectetuer id, vulputate a, magna. Donec vehicula augue eu neque. Pellentesque habitant morbi tristique senectus et netus et malesuada fames ac turpis egestas. Mauris ut leo. Cras viverra metus rhoncus sem. Nulla et lectus vestibulum urna fringilla ultrices. Phasellus eu tellus sit amet tortor gravida placerat. Integer sapien est, iaculis in, pretium quis, viverra ac, nunc. Praesent eget sem vel leo ultrices bibendum. Aenean faucibus. Morbi dolor nulla, malesuada eu, pulvinar at, mollis ac, nulla. Curabitur auctor semper nulla. Donec varius orci eget risus. Duis nibh mi, congue eu, accumsan eleifend, sagittis quis, diam. Duis eget orci sit amet orci dignissim rutrum.

1. Introduction

Floating offshore wind turbines (FOWTs) have been the subject of numerous studies due to the possibility of exploiting the vast wind resources located in deep waters. As an emerging technology, the growth of the wind energy industry depends on FOWTs achieving more competitive costs, which has pushed for larger rotors and new designs for both floaters and moorings.

Since FOWTs are complex structures, their design requires the evaluation of performance and structural integrity for a myriad of environmental conditions (wind, wave, current, among others) and operating conditions (power production, normal shut down, fault conditions, etc.). Due to their intricate dynamics, this procedure requires modeling software capable of accounting for the couplings between aerodynamics, hydrodynamics, controls, moorings and structural behavior, which are commonly referred as aero-hydro-servo-elastic tools. A substantial effort has been made to validate these software, as exemplified by the OC3 (Jonkman and Musial, 2010), OC4 (Robertson et al., 2014) and OC5 (Robertson et al., 2017) projects, but this is still an ongoing development.

In fact, the experiments required to validate the numerical tools, usually performed in model scale, are far from an easy task, for it is impossible to keep all the dimensionless parameters that describe the different physical aspects of the problem. For instance, while the scaling of the waves requires that the Froude number ($\mathrm{Fr} = U^2/(gL)$, with U a characteristic speed, L a characteristic length and g the gravitational acceleration) be conserved, the aerodynamic loads are governed by the Reynolds number ($\mathrm{Re} = UL/\nu$, with ν the kinematic viscosity). To work around this incompatibility, some alternatives have been tried to perform tests with both wind and waves, and a thorough review of experimental techniques for doing so can be found in Otter et al. (2022). For instance, some works have used a Froude scaled rotor with the wind generated by fans at higher speeds than the scaled ones, so that the correct rotor thrust was obtained (Martin et al., 2014; Skaare et al., 2007; Mortensen et al., 2018); however, this approach has the downside that either the tip speed ratio (TSR) or the excitation frequencies are not preserved. Others have employed performance scaled rotors (Goupee et al., 2014; de Ridder et al., 2014; Bredmose et al., 2017), in the sense that the rotors were redesigned with geometrically modified airfoils to compensate for the low Reynolds number obtained in a Froude scale experiment.

A different line of thought is adopted by the so-called hybrid tests, in which either the aerodynamic or hydrodynamic forces are computed numerically and applied to the FOWT instead of being a consequence of the physical interaction of the hull/rotor with the waves/wind. The present work deals with the case in which the experiments are performed

*Corresponding author.
lucas.carmo@usp.br (L.H.S. Carmo)
ORCID(s): 0000-0001-8744-1391 (L.H.S. Carmo); 0000-0003-2621-9644 (P.C.d. Mello); 0000-0002-7453-8650 (R.M. Monaro); 0000-0002-1879-5468 (A.N. Simos)

in a wave basin, so the waves are still generated physically, while the aerodynamic forces are replaced by a numerical model. This approach, called software-in-the-loop (SIL), was first employed by Azcona et al. (2014), who used a single ducted propeller in place of the turbine rotor to emulate the aerodynamic thrust, while the aerodynamic forces acting on the other degrees of freedom were disregarded. In a nutshell, it consists in measuring the motions of the FOWT model, which is floating in the wave basin, and feeding these motions to the software, in which the aerodynamic forces acting on a virtual rotor under the action of a virtual wind are computed numerically – in that case and in the present work, using Blade Element Momentum Theory (BEMT). Finally, the rotational speed of the fan is controlled in order to provide the required thrust. The fact that this procedure happens in real time and taking into account the motions of the structure makes it simple to synchronize wave elevation and wind loads, besides allowing the modeling of aerodynamic damping and turbine control. In subsequent works, the SIL method has been applied with multi-propeller actuators in order to model not only the aerodynamic thrust, but also the forces and moments along the other degrees of freedom (Pires et al., 2020; Otter et al., 2020).

Alternatively, some works have employed cables pulled by winches instead of fans to emulate the aerodynamic loads (Sauder et al., 2016; Bachynski et al., 2016; Thys et al., 2018), while the option of performing the experiment in a wind tunnel whilst the hydrodynamics of the FOWT is computed numerically is discussed by Bayati et al. (2018) and Belloli et al. (2020). However, the SIL method proposed by Azcona et al. (2014) has the advantage of being the simplest option in terms of required equipment for a wave basin such as the one from the Numerical Offshore Tank of the University of São Paulo (TPN-USP).

Besides improving the capabilities of TPN-USP to be able to perform experimental tests of FOWTs under the concomitant action of wind and waves, this work aims at validating the numerical models that were used during the design of a FOWT concept developed in the context of a joint research project with Petrobras (Mas-Soler et al., 2022), which illustrated in Figure 1 and goes by the provisional name FOWTC. Due to these two different objectives, this paper is divided into two parts:

Figure 1: Illustration of the FOWTC concept.

i. In the first part, which is provided in Section 4, the experiments are used to verify aspects of the hydrodynamics of the floater (which is the part that is physically modeled in the tests) that the numerical analyses should take into account. More specifically, a numerical model as close as possible to the conditions of the experiment is built with OpenFAST (Jonkman and Buhl, 2005) and WAMIT (WAMIT, 2004), and this model is used to demonstrate the importance of drag forces on the pontoons and of second-order wave forces in both the horizontal and vertical degrees of freedom (dofs). The impact of considering the mean hull inclination induced by the wind for computing the radiation/diffraction coefficients in WAMIT is also assessed, and it is shown that this effect is negligible;

ii. In the second part, given in Section 5, the objective is to investigate the relevance of two physical aspects that were not included in the aerodynamic modeling adopted in the tests. The first of them is that the SIL implementation employed a fan assembly that was only able to apply the aerodynamic thrust, thus loads in the other dofs were not present in the model; the other aspect is that blade elasticity was not considered in this first version of the software, a point that is planned to be addressed in future versions. In order to verify the impact of these simplifications, the numerical models that are validated in the first part of the paper are compared with additional OpenFAST models that consider both blade elasticity and the aerodynamic forces on the six dofs.

Before presenting the two topics above, Section 2 describes the prototype and experimental setup, including the SIL method and its limitations, while Section 3 describes the numerical models considered in this work.

2. Description of the prototype and the experimental setup

Falar que foi feito no TPN e dar as principais dimensoes do tanque.

2.1. Main properties of the FOWT

- Caracteristicas da FOWT, RNA, ancoragem

2.2. Software-in-the-loop approach for aerodynamic loads

Tem que incluir o controle. Adicionar alguns resultados de teste de bancada

2.3. Limitations of the experiment

2.4. Environmental conditions

- Condições de onda e vento

3. Numerical models

The wave forces are considered in OpenFAST by a combination of radiation/diffraction forces, taken into account using Cummins' approach (Cummins, 1962; Ogilvie, 1964) with frequency-domain coefficients computed with WAMIT (version 7.0.1), and the quadratic drag from Morison's equation. Concerning the former, one of the main questions about the numerical modeling of the experiments was wether the mean hull inclination caused by the wind should be considered when solving the radiation/diffraction problem. Indeed, one of the main hypothesis of the Boundary Element Method behind WAMIT is that the body oscillates around a mean position, but it is not clear at first how important the few degrees of inclination induced by the wind are.

For that reason, a different set of radiation/diffraction coefficients (i.e. first- and second-order wave forces, added mass and potential damping) was computed for each wind condition, using low order meshes with different inclinations that were determined by experimentally measuring the inclination of the model under the action of constant wind in calm waters. Since this is a somewhat cumbersome procedure, it is important to assess whether it is worth the cost, so all the OpenFAST simulations were performed twice: once with radiation/diffraction coefficients obtained using the inclined mesh, and once with coefficients from an even keel mesh. One of the inclined meshes (ESPECIFICAR) and the even keel mesh are illustrated in Figures XX, while the differences between the results obtained with them are discussed in Section 4.3.

4. Reproducing the experiments with numerical models

As outlined in Section 1, the purpose of this section is to discuss the relevance of three specific points concerning the hydrodynamic modeling in the numerical simulations, in light of the experimental results: the drag forces on the pontoons (Section 4.1); the need for second-order wave forces not only for the horizontal motions, but also for the vertical dofs (Section 4.2); and whether the mean hull inclination induced by the wind needs to be considered in the solution of the radiation/diffraction problem (Section 4.3). After these aspects have been discussed, Section 4.4 summarizes the main results to show the adherence between the numerical simulations and the experiment.

4.1. The need for drag forces on the pontoons

The first point concerns the drag forces on the pontoons of the hull, which are relevant not only due to the damping that they introduce, but also because drag is and important forcing term for this type of floater. These forces are modeled in OpenFAST using Morison elements, but since the current version of the software includes only circular elements, the source code was modified to account for elements with rectangular cross section. In this modified version, the drag forces per unit length are given by:

$$f_{Dx} = \frac{1}{2}\rho C_{Dx} D_x ||\mathbf{u}|| u_x$$
$$f_{Dy} = \frac{1}{2}\rho C_{Dy} D_y ||\mathbf{u}|| u_y \quad (1)$$

where $\mathbf{u} = u_x\mathbf{e}_1 + u_y\mathbf{e}_2$ is the relative fluid velocity (i.e. the difference between fluid velocity and local body velocity); $\mathbf{e}_1$ and $\mathbf{e}_2$ are the unit vectors directed along the local x and y axes, which are normal to the lateral faces of the rectangular cylinder; C_{Dx} and C_{Dy} are the drag coefficients in each direction; and D_x and D_y are the sides of the rectangle.

The drag coefficients in each direction are obtained by matching numerical decays in surge and heave with their experimental counterparts, as illustrated in Figures 2 and 3. These decays were performed with the complete setup of the experiment, hence with both the mooring lines and the umbilical cables needed by the SIL method, but without either wind or waves. In the right side of each graph is presented a PQ-analysis (Burmester et al., 2020), in which the slope of the curve corresponds to the quadratic damping, while the intersection with the y axis is proportional to the linear damping. It turns out that the latter, which is mostly due to wave radiation, is negligible, being relevant only when the amplitude of motion is very small (note that the experiment provides a negative value for the linear heave damping, which is clearly not physical and a consequence of the small values involved). On the other hand, the quadratic damping, which is obtained considering the drag coefficients summarized in Table 1, is within the range of values measured in the experiments (3 repetitions in surge and 7 in heave), as shown in Table 2 (a complete set of decay results is given in Table 5). Note that it would be impossible to match the damping levels in both dofs simultaneously if the pontoons were modeled using circular Morison elements, since both D and C_D are different for each direction.

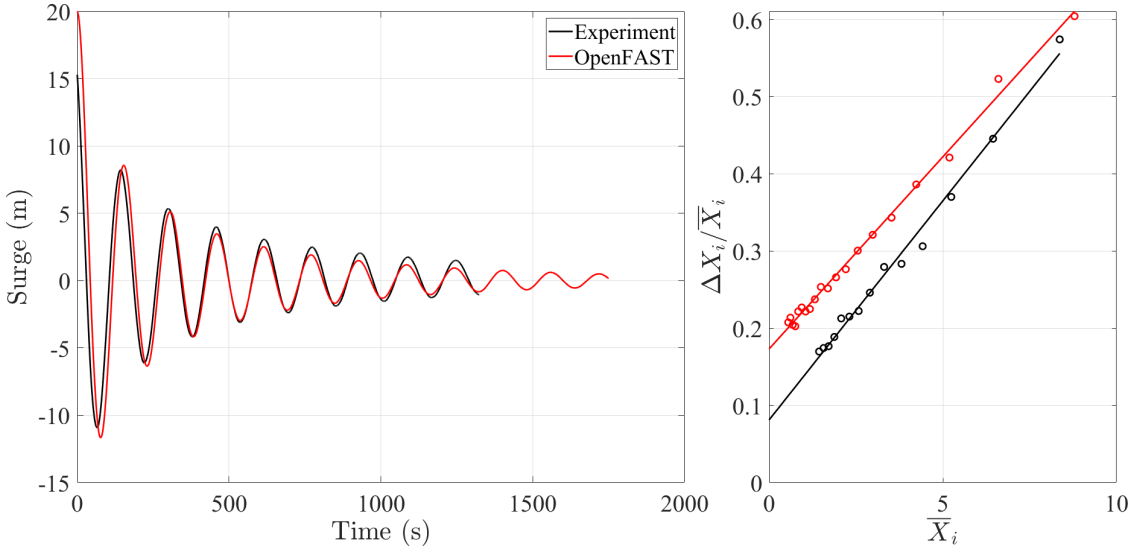

Figure 2: Comparison of numerical and experimental surge decays.

Though the drag coefficients obtained from decay tests are not necessarily the same required by simulations considering waves, the values provided in Table 1 have led to good results for all the wave and wind conditions analyzed in this work, as will be shown in Section 4.4. For now, a single test case is enough to illustrate the influence of the drag forces. For that, Figures 4 and 5 present the surge and heave motions of the FOWT under the action of the IRR-I1 wave ($T_P = 14.5$ m and $H_S = 9.3$ m) and an incidence of -10° (following the same convention as HydroDyn), without wind effects. To evidence the importance of the drag forces, the plots include results of simulations performed with circular

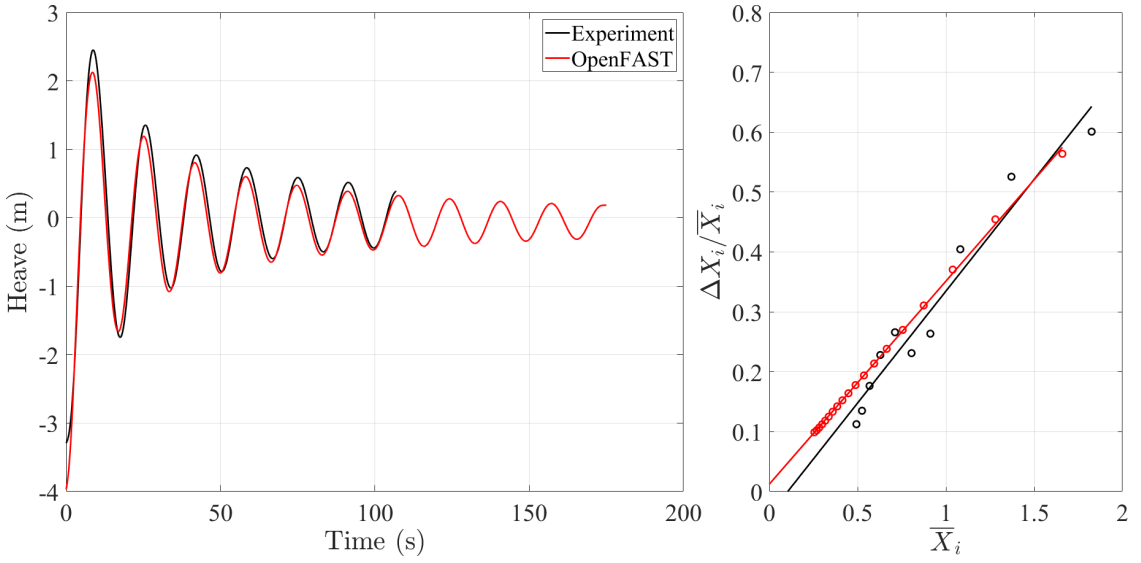

Figure 3: Comparison of numerical and experimental heave decays.

Table 1
Resulting drag coefficient for each Morison element and its main dimensions.

	Length	Diameter	C_D
Central column	18.6	14.1	0.61
Offset columns	18.6	17.0	0.61
Pontoons - Vertical	23.0	17.0	12.00
Pontoons - Horizontal	23.0	6.0	2.50

Table 2
Comparison between the experimental and numerical values of the nondimensional quadratic drag coefficient (B_Q/M) obtained in the surge/heave decays.

	Experiment	OpenFAST
Surge	0.021 ± 0.002	0.019
Heave	0.145 ± 0.022	0.127

Morison elements calibrated for the opposite dof, i.e. the results labeled "OpenFAST - Circ. pontoon S" presented in the heave graphs correspond to a circular pontoon with $D = 6.0$ m and $C_D = 2.50$, which are the values obtained from the surge decays; conversely, "OpenFAST - Circ. pontoon H" correspond to a circular pontoon calibrated using the heave decays.

The first set of graphs, Figure 4, shows that the difference in drag models has a significant impact on the surge motion only around its resonance frequency, which is expected due to the different damping levels. However, the slow surge motion is underpredicted even by the OpenFAST model with rectangular pontoons and drag coefficients calibrated from decay tests. The main hypothesis is that this is related to an underprediction of the low-frequency force rather than an overprediction of damping, following the findings by Wang et al. (2022), who showed that a third-order force that arises from computing the drag loads considering the instantaneous wave elevation (as opposed to the approach considered in this work, which integrates drag loads up to the mean water level) explained the underprediction of the slow surge motion reported by Robertson et al. (2017).

The impact of drag on heave is more critical than observed for surge, as illustrated in Figure 5. In this case, it acts not only by damping the resonant response around 16.5 s (0.061 Hz), but also as a relevant forcing term around 15 s (0.067 Hz). This is made clear by the Heave RAOs plotted on the bottom right of the same figure, which show that the

response predicted by WAMIT is almost zero at 15 s, a consequence of the force obtained with potential flow being null close to that period, while the result with OpenFAST considering the rectangular pontoon adheres very well to the experiment. This means that it would not be possible to model this behavior by tuning an external quadratic damping coefficient, as neglecting this forcing term would lead to important underpredictions of the motions.

Still about heave, it is noteworthy that a single set of drag coefficients, obtained from such a simple procedure as a decay test and using an equally simple approach as Morison's equation, was able to model pretty well both the situation in which drag acts by damping the motion and the one in which it plays the role of a forcing term.

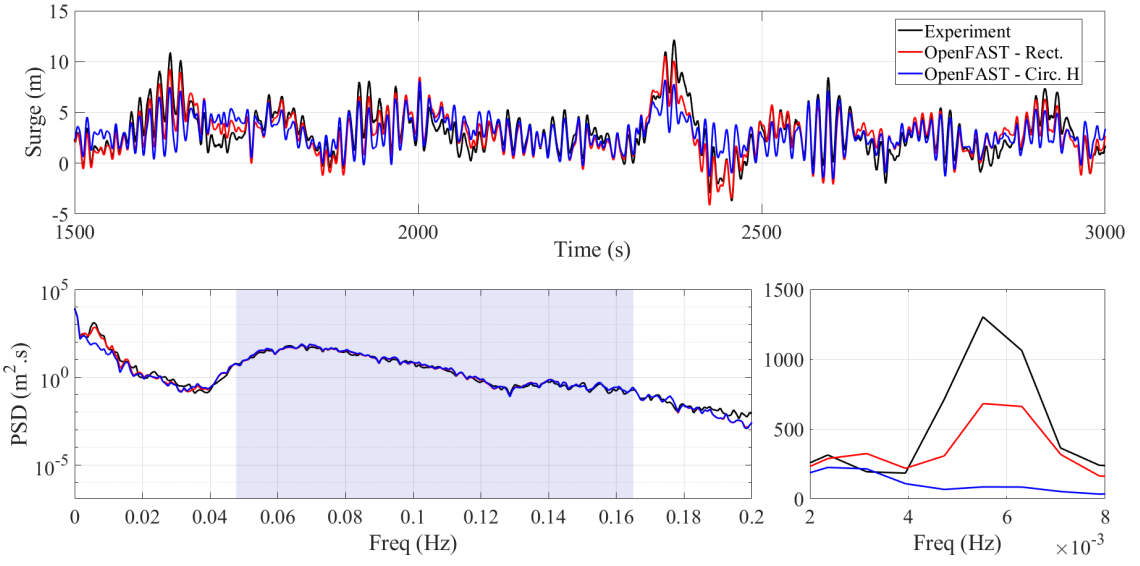

Figure 4: Illustration of the influence on surge motions of the drag forces on the pontoons (IRR-I1 wave, incidence of -10°, without wind effects). The bottom right plot is a zoom in linear scale of the PSD around the resonance frequency of surge (about 0.006 Hz). The range of frequencies corresponding to the incoming waves is shaded in blue.

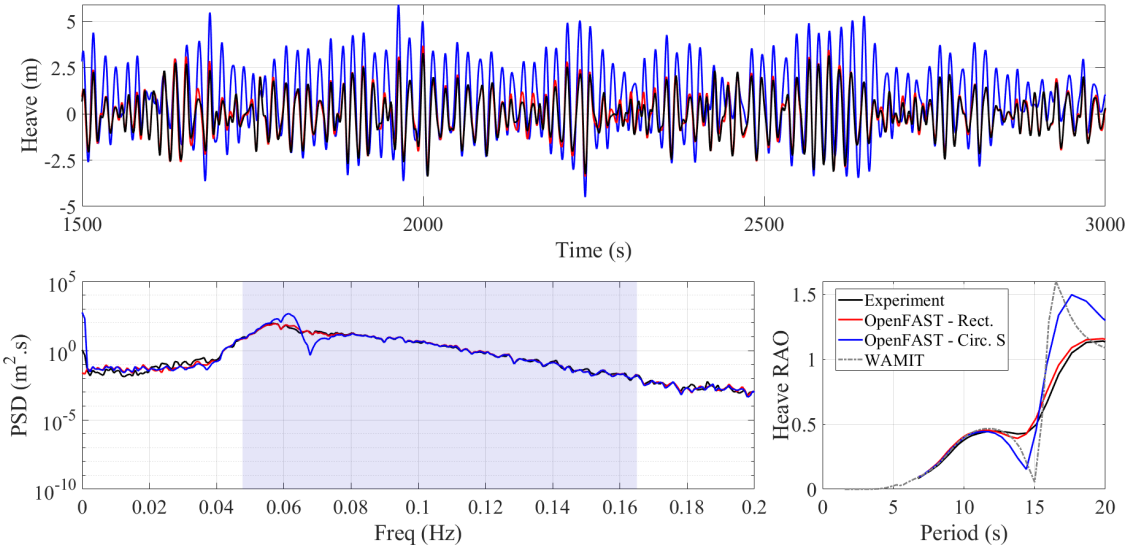

Figure 5: Illustration of the influence on heave motions of the drag forces on the pontoons (IRR-I1 wave, incidence of 60°, without wind effects). The range of frequencies corresponding to the incoming waves is shaded in blue.

4.2. The importance of second-order wave forces for vertical motions

The relevance of low-frequency second-order wave forces on the dynamics of FOWTs is well known and documented in the literature (Coulling et al., 2013; Gueydon et al., 2014; Lopez-Pavon et al., 2015; Robertson et al., 2017; Simos et al., 2018), and this section is an addition to this ongoing discussion in order to emphasize the importance of this force component not only for the horizontal motions of the floater, but also for the vertical degrees of freedom.

There are a number of approaches and simplifications that can be adopted to compute second-order forces. Due to its simplicity, the first procedure that was tested in this study was to compute the slow-drift forces using Newman's approximation (Newman, 1974), but for the horizontal degrees of freedom only. This is a very simple approach because it only requires the mean forces/moments, which do not depend on the solution of the second-order problem, and the integrations are performed based on conservation of momentum, which is far less strict in terms of mesh convergence. For the reader familiar with WAMIT, this corresponds to the .8 files.

This approach is usually enough for the analysis of floating systems in deep waters and for which surge, sway and yaw (typically with low natural frequencies) are the only degrees of freedom that present significant slow motions. Unfortunately, this is not the case for most FOWTs, including the one analyzed in this study, and analyzes considering complete sets of QTF (Quadratic Transfer Function) matrices are required. However, as one of the objectives of this work is to analyze the impact of mean hull inclination on the solution of the radiation/diffraction problem (discussed ahead in Section 4.3), it would be unfeasible to compute the completes QTFs for all the different conditions. For this reason, an intermediate approach is adopted in which Newman's approximation is used with a mixed mean drift file in which the horizontal degrees of freedom (surge, sway and yaw) are computed with conservation of momentum (WAMIT .8 file) while the vertical motions (heave, roll and pitch) are calculated using pressure integration (WAMIT .9 file). The advantage is that the convergence of pressure integration is more complicated for the horizontal dofs than for the vertical dofs due to the larger gradient near the free-surface, so this mixed procedure saves computational time.

The results obtained for the pitch motion with each of these approaches are illustrated in Figure 8[1], considering the same wave as the previous section (IRR-I1 wave, i.e. $T_P = 14.5$ m, $H_S = 9.3$ m and an incidence of -10°). It is clear that neglecting the slow-pitch forces (the simulations considering the .8 file alone) leads to an important underprediction of pitch motion: the predicted maximum angle of 2.0° is considerably lower than the value of 4.0° measured in the experiments. The results improve significantly when Newman's approximation is employed considering vertical mean forces (mixed .8 and .9 file), with the simulations providing a maximum angle of 4.0°.

4.3. The impact of mean hull inclination when computing radiation/diffraction coefficients

As mentioned in Section 3, one of the objectives of this work is to assess the impact of considering the mean hull inclination caused by the wind when solving the radiation/diffraction problem. Figure X, which summarizes in a boxplot the differences in the maxima obtained for each of the quantities analyzed in the previous sections for all the irregular waves, shows that this is not the case: in fact, the differences are ..... (falar também que a diferença é ainda mais irrelevante quando se pensa na tabela de extremos)

Mostrar um gráfico comparando as estatísticas calculadas c/ inclinação e sem.

As a more in-depth example, Figure X presents the time series and PSD's of roll and pitch motion obtained for the FOWT under the combined action of the IRR12 sea ($H_S = 4.44$ m, $T_P = 11.34$ s and incidence of -10°) and the turbulent wind condition (mean wind speed 10.59 s and TI = 12%) with an incidence of 47°, which is schematized in the same figure. This case was chosen for being the one that presented the largest difference in the horiontal acceleration at the nacelle, with the model considering an inclined mesh (denoted by IC) predicting a maximum horizontal acceleration of 0.85 m/s^2 and the one with an even keel mesh (denoted by EK) providing 0.74 m/s^2, which is actually closer to the experimental value of 0.64 m/s^2.

Mostrar gráfico de série temporal do que deu a maior diferença e explicar usando RAO e o .3

In fact, this could be anticipated by looking directly at the radiation/diffraction coefficients that are imported by OpenFAST. These are illustrated by Figure X (first-order diffraction forces), Figure X (mean drift force) and Figure X (added mass and potential damping). For conciseness, only the mesh with the largest inclination (dizer qual é aqui, i.e. p/ qual vento, e qual é a inclinação) and only one wave incidence (45°) is plotted, and the results for sway and roll are omitted because they are qualitatively the same as surge and pitch.

Mostrar gráficos das forças

It is worth pointing out that only the impact on the radiation/diffraction coefficients was assessed, and it is possible that hull inclination may be important to effects related to real flow phenomena, such as drag forces.

[1] The importance of slow surge forces was already made clear in Section 4.1 by the resonant motion presented in Figure 4

4.4. Main results

Explicar o procedimento adotado para processar a grande quantidade de ondas, que é baseado nas estatísticas. Mostrar tabela com períodos naturais e níveis de amortecimentos + tabela de resumo das estatísticas p/ ondas irregulares.

Ilustrar c/ gráficos de séries temporais e espectros de casos selecionados (tem que ter a aerodinâmica p/ mostrar que o rotor tá funcionando) + gráfico do máximo e média (tentar colocar um monte na mesma figura)

5. The impact of rotor simplifications adopted in the model tests

- Comparar resultados das simulações nas condições reais e identificar diferenças pro modelo que é mais próximo do ensaio.

- Usar simulações intermediárias p/ explicar essas diferenças

6. Conclusions

CRediT authorship contribution statement

Lucas H. S. Carmo: Conceptualization, Methodology, Software, Validation, Formal analysis, Writing – original draft. **Pedro C. de Mello:** Experiments. **Renato M. Monaro:** Experiments. **Alexandre N. Simos:** Conceptualization, Formal analysis, Writing – review, Supervision.

Declaration of competing interest

The authors declare that they have no known competing financial interests or personal relationships that could have appeared to influence the work reported in this paper.

Acknowledgments

This study was financed in part by the Coordenação de Aperfeiçoamento de Pessoal de Nível Superior - Brasil (CAPES) - Finance Code 001. Alexandre Simos thanks the Brazilian National Council for Scientific and Technological Development - CNPq - for his research grant (# 306342/2020-0).

References

Azcona, J., Bouchotrouch, F., González, M., Garciandía, J., Munduate, X., Kelberlau, F., Nygaard, T.A., 2014. Aerodynamic thrust modelling in wave tank tests of offshore floating wind turbines using a ducted fan, in: Journal of Physics: Conference Series, IOP Publishing. p. 012089.

Bachynski, E.E., Thys, M., Sauder, T., Chabaud, V., Sæther, L.O., 2016. Real-time hybrid model testing of a braceless semi-submersible wind turbine: Part II—Experimental results, in: International Conference on Offshore Mechanics and Arctic Engineering, American Society of Mechanical Engineers. p. V006T09A040.

Bayati, I., Facchinetti, A., Fontanella, A., Giberti, H., Belloli, M., 2018. A wind tunnel/HIL setup for integrated tests of Floating Offshore Wind Turbines, in: Journal of Physics: Conference Series, IOP Publishing. p. 052025.

Belloli, M., Bayati, I., Facchinetti, A., Fontanella, A., Giberti, H., La Mura, F., Taruffi, F., Zasso, A., 2020. A hybrid methodology for wind tunnel testing of floating offshore wind turbines. Ocean Engineering 210, 107592.

Bredmose, H., Lemmer, F., Borg, M., Pegalajar-Jurado, A., Mikkelsen, R.F., Larsen, T.S., Fjelstrup, T., Yu, W., Lomholt, A.K., Boehm, L., et al., 2017. The Triple Spar campaign: Model tests of a 10mw floating wind turbine with waves, wind and pitch control. Energy Procedia 137, 58–76.

Burmester, S., Vaz, G., Gueydon, S., el Moctar, O., 2020. Investigation of a semi-submersible floating wind turbine in surge decay using CFD. Ship Technology Research 67, 2–14.

Coulling, A., Goupee, A., Robertson, A., Jonkman, J., 2013. Importance of second-order difference-frequency wave-diffraction forces in the validation of a FAST semi-submersible floating wind turbine model, in: 32nd International Conference on Ocean, Offshore and Arctic Engineering, ASME. p. V008T09A019.

Cummins, W.E., 1962. The impulse response function and ship motions. Technical Report. Technical Report 1661, David Taylor Model Basin.

Goupee, A.J., Koo, B.J., Kimball, R.W., Lambrakos, K.F., Dagher, H.J., 2014. Experimental comparison of three floating wind turbine concepts. Journal of Offshore Mechanics and Arctic Engineering 136.

Gueydon, S., Duarte, T., Jonkman, J., 2014. Comparison of second-order loads on a semisubmersible floating wind turbine, in: 33th International Conference on Ocean, Offshore and Arctic Engineering, ASME. p. V09AT09A024.

Jonkman, J., Buhl, M., 2005. FAST User's Guide. Technical Report. National Renewable Energy Laboratory (NREL). Golden, CO, USA.

Jonkman, J., Musial, W., 2010. Offshore Code Comparison Collaboration (OC3) for IEA Wind Task 23 offshore wind technology and deployment. Technical Report. National Renewable Energy Lab.(NREL), Golden, CO (United States). Golden, CO, USA.

Lopez-Pavon, C., Watai, R.A., Ruggeri, F., Simos, A., Souto-Iglesias, A., 2015. Influence of wave induced second-order forces in semisubmersible FOWT mooring design. Journal of Offshore Mechanics and Arctic Engineering 137.

Martin, H.R., Kimball, R.W., Viselli, A.M., Goupee, A.J., 2014. Methodology for wind/wave basin testing of floating offshore wind turbines. Journal of Offshore Mechanics and Arctic Engineering 136.

Mas-Soler, J., do Amaral, G.A., da Silva, L.Z., Malta, E.B., Carmo, L.H.S., Ruggeri, F., Simos, A.N., 2022. A parametric optimization approach for the initial design of FOWT's substructure and moorings in brazilian deep-water fields, in: Journal of Physics: Conference Series, IOP Publishing. p. 012025.

Mortensen, S.M., Laugesen, K., Jensen, J.K., Jessen, K., Soltani, M., 2018. Experimental verification of the hydro-elastic model of a scaled floating offshore wind turbine, in: 2018 IEEE Conference on Control Technology and Applications (CCTA), IEEE. pp. 1623–1630.

Newman, J.N., 1974. Second-order, slowly-varying forces on vessels in irregular waves, in: Proc. Int. Symp. Dynamics of Marine Vehicles and Structures in Waves, Mechanical Engineering Publications Ltd., London, UK.

Ogilvie, T.F., 1964. Recent progress toward the understanding and prediction of ship motions, in: 5th Symposium on Naval Hydrodynamics, ONR, Bergen, Norway.

Otter, A., Murphy, J., Desmond, C., 2020. Emulating aerodynamic forces and moments for hybrid testing of floating wind turbine models, in: Journal of Physics: Conference Series, IOP Publishing. p. 032022.

Otter, A., Murphy, J., Pakrashi, V., Robertson, A., Desmond, C., 2022. A review of modelling techniques for floating offshore wind turbines. Wind Energy 25, 831–857.

Pires, O., Azcona, J., Vittori, F., Bayati, I., Gueydon, S., Fontanella, A., Liu, Y., De Ridder, E., Belloli, M., Van Wingerden, J., 2020. Inclusion of rotor moments in scaled wave tank test of a floating wind turbine using SIL hybrid method, in: Journal of Physics: Conference Series, IOP Publishing. p. 032048.

de Ridder, E.J., Otto, W., Zondervan, G.J., Huijs, F., Vaz, G., 2014. Development of a scaled-down floating wind turbine for offshore basin testing, in: International Conference on Offshore Mechanics and Arctic Engineering, American Society of Mechanical Engineers. p. V09AT09A027.

Robertson, A., Jonkman, J., Vorpahl, F., Popko, W., Qvist, J., Frøyd, L., Chen, X., Azona, J., Uzunoglu, E., Soares, C.G., Luan, C., Yutong, H., Pengcheng, F., Yde, A., Larsen, T., Nichols, J., Buils, R., Lei, L., Nygaard, T., Manolas, D., Heege, A., Vatne, S., Ormberg, H., Duarte, T., Godreau, C., Hansen, H., Nielsen, A., Riber, H., Le Cunff, C., Beyer, F., Yamaguchi, A., Jung, K., Shin, H., Shi, W.and Park, H., Alves, M., Guérinel, M., 2014. Offshore Code Comparison Collaboration Continuation within IEA Wind Task 30: Phase II results regarding a floating semisubmersible wind system, in: 33rd International Conference on Ocean, Offshore and Arctic Engineering, ASME, San Francisco, CA, USA.

Robertson, A., Wendt, F., Jonkman, J., Popko, W., Dagher, H., Gueydon, S., Qvist, J., Vittori, F., Azcona, J., Uzunoglu, E., Soares, C., Harries, R., Yde, A., Galinos, C., Hermans, K., de Vaal, J., Bozonnet, P., Bouy, L., Bayati, I., Bergua, R., Galvan, J., Mendikoa, I., Sanchez, C., Shin, H., Oh, S., Molins, C., Debruyne, Y., 2017. OC5 project phase II: Validation of global loads of the DeepCwind floating semisubmersible wind turbine. Energy Procedia 137, 38 – 57. 14th Deep Sea Offshore Wind R&D Conference, EERA DeepWind.

Sauder, T., Chabaud, V., Thys, M., Bachynski, E.E., Sæther, L.O., 2016. Real-time hybrid model testing of a braceless semi-submersible wind turbine: Part I—The hybrid approach, in: International Conference on Offshore Mechanics and Arctic Engineering, American Society of Mechanical Engineers. p. V006T09A039.

Simos, A.N., Ruggeri, F., Watai, R.A., Souto-Iglesias, A., Lopez-Pavon, C., 2018. Slow-drift of a floating wind turbine: An assessment of frequency-domain methods based on model tests. Renewable energy 116, 133–154.

Skaare, B., Hanson, T.D., Nielsen, F.G., Yttervik, R., Hansen, A.M., Thomsen, K., Larsen, T.J., 2007. Integrated dynamic analysis of floating offshore wind turbines, in: European wind energy conference and exhibition, Hamburg, Germany. pp. 1929–1939.

Thys, M., Chabaud, V., Sauder, T., Eliassen, L., Sæther, L.O., Magnussen, Ø.B., 2018. Real-time hybrid model testing of a semi-submersible 10MW floating wind turbine and advances in the test method, in: International Conference on Offshore Mechanics and Arctic Engineering, American Society of Mechanical Engineers. p. V001T01A013.

WAMIT, I., 2004. WAMIT User Manual - Versions 6.2, 6.2PC, 6.2S, 6.1S-PC. Chestnut Hill, MA, USA.

Wang, L., Robertson, A., Jonkman, J., Yu, Y.H., 2022. OC6 phase I: Improvements to the OpenFAST predictions of nonlinear, low-frequency responses of a floating offshore wind turbine platform. Renewable Energy 187, 282–301.